## Supplemental Information

# Identification of Early RET+ Deep Dorsal Spinal Cord Interneurons in Gating Pain

Lian Cui[1#], Xuerong Miao[2#], Lingli Liang[2], Ishmail Abdus-Saboor[1], William Olson[1], Michael S Fleming[1], Minghong Ma[1], Yuan-Xiang Tao[2]*, Wenqin Luo[1]*

## Inventory of Supplemental Information

1. Supplemental Figures

**1. Supplemental Figures**

Figure S1

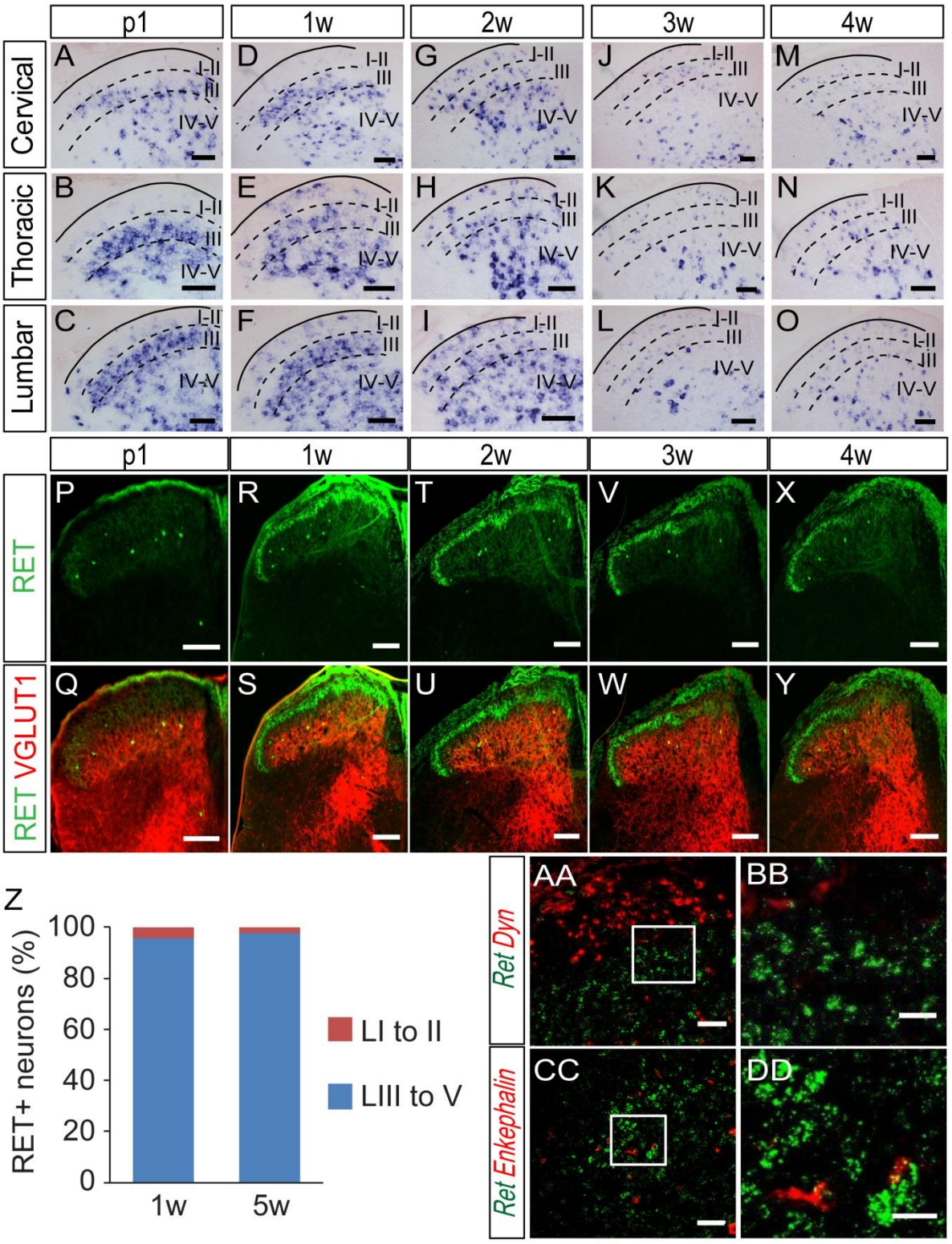

Figure S2

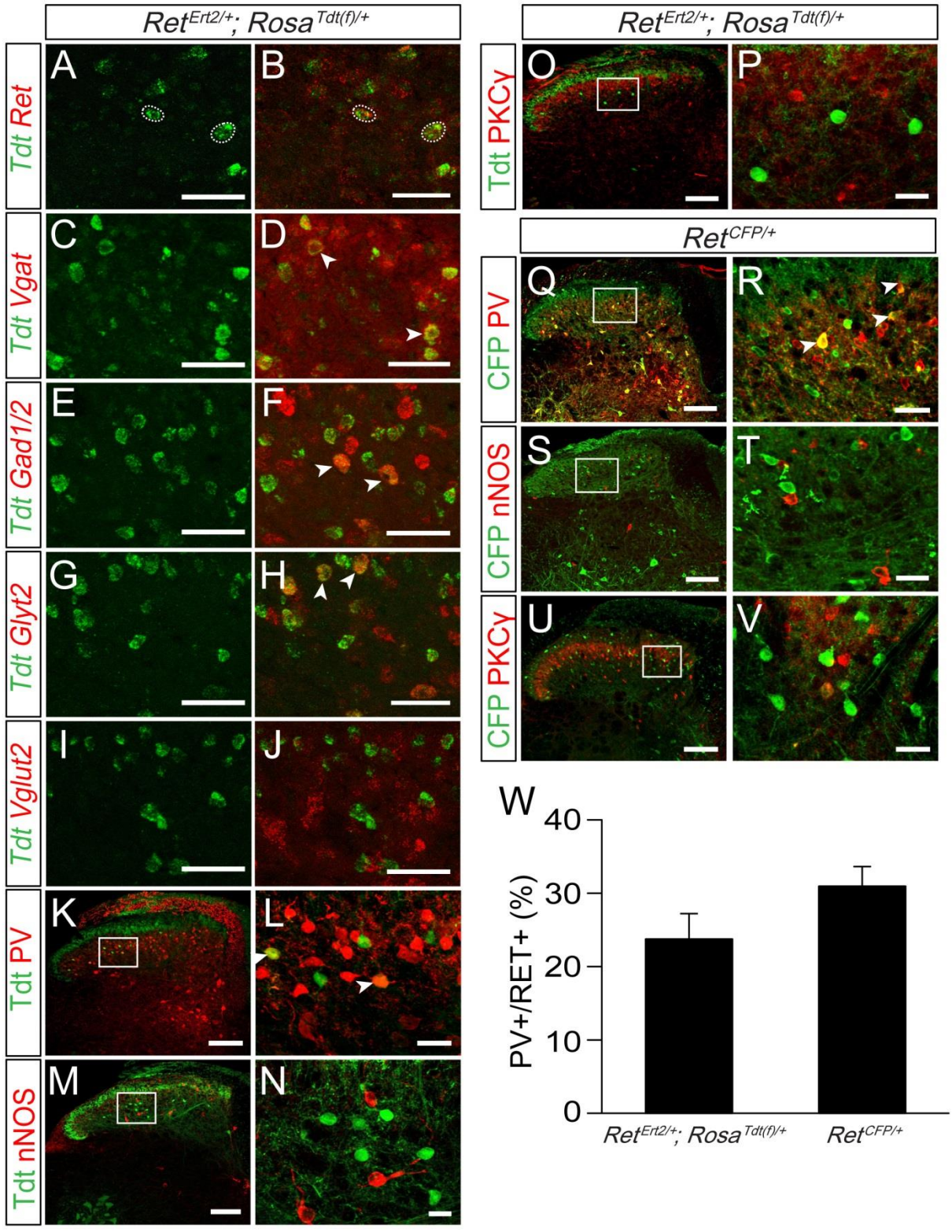
Ret^Ert2/+; Rosa^Tdt(f)/+
Tdt Ret
A
B
Tdt Vgat
C
D
Tdt Gad1/2
E
F
Tdt Glyt2
G
H
Tdt Vglut2
I
J
Tdt PV
K
L
Tdt nNOS
M
N
Ret^Ert2/+; Rosa^Tdt(f)/+
Tdt PKCγ
O
P
Ret^CFP/+
CFP PV
Q
R
CFP nNOS
S
T
CFP PKCγ
U
V
W
PV+/RET+ (%)
40
30
20
10
0
Ret^Ert2/+; Rosa^Tdt(f)/+
Ret^CFP/+

Figure S3

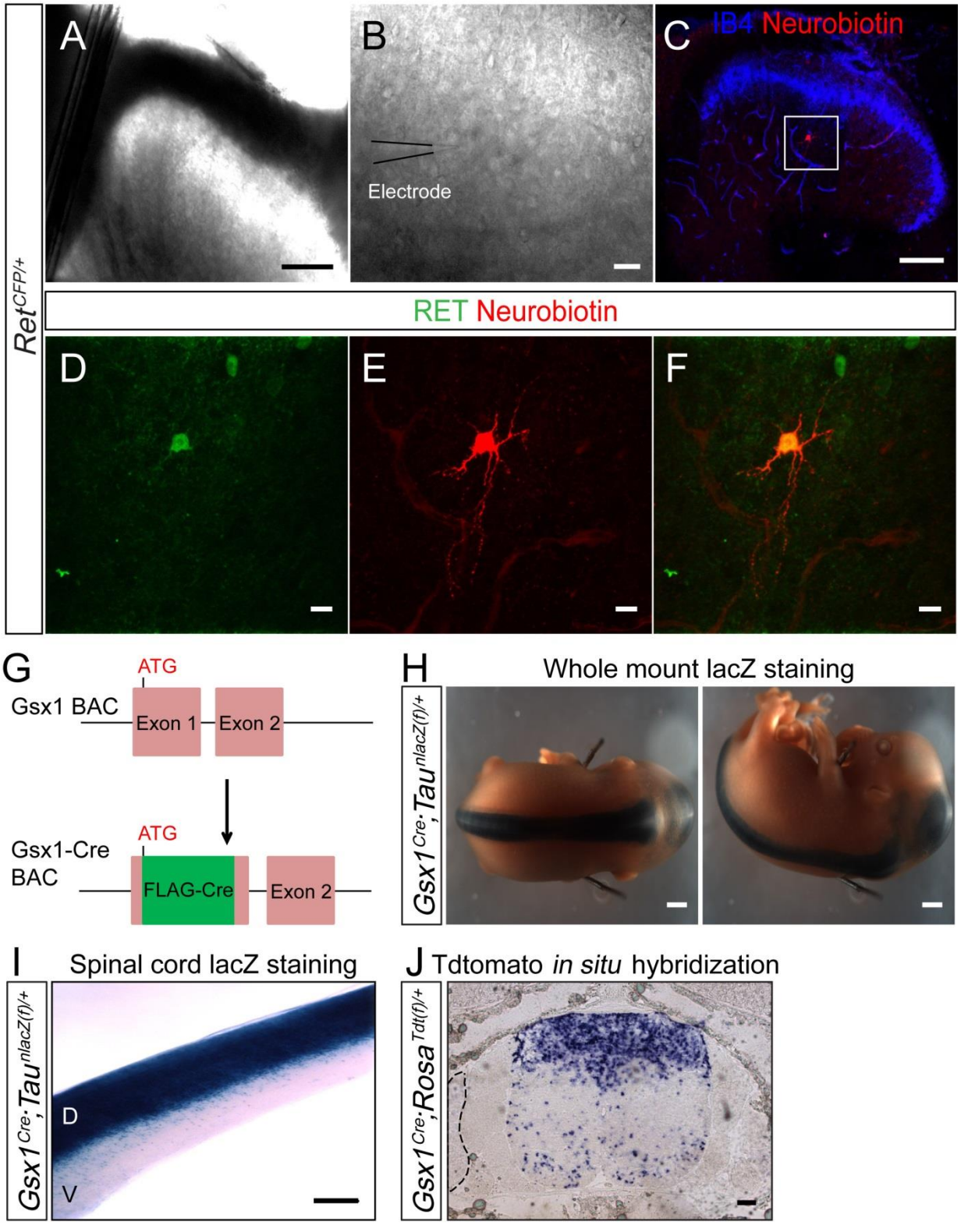
A
B
C
IB4 Neurobiotin
Electrode
Ret^CFP/+
RET Neurobiotin
D
E
F
G
ATG
Gsx1 BAC
Exon 1
Exon 2
ATG
Gsx1-Cre BAC
FLAG-Cre
Exon 2
H
Whole mount lacZ staining
Gsx1^Cre;Tau^nlacZ(f)/+
I
Spinal cord lacZ staining
Gsx1^Cre;Tau^nlacZ(f)/+
D
V
J
Tdtomato in situ hybridization
Gsx1^Cre;Rosa^Tdt(f)/+

Figure S4

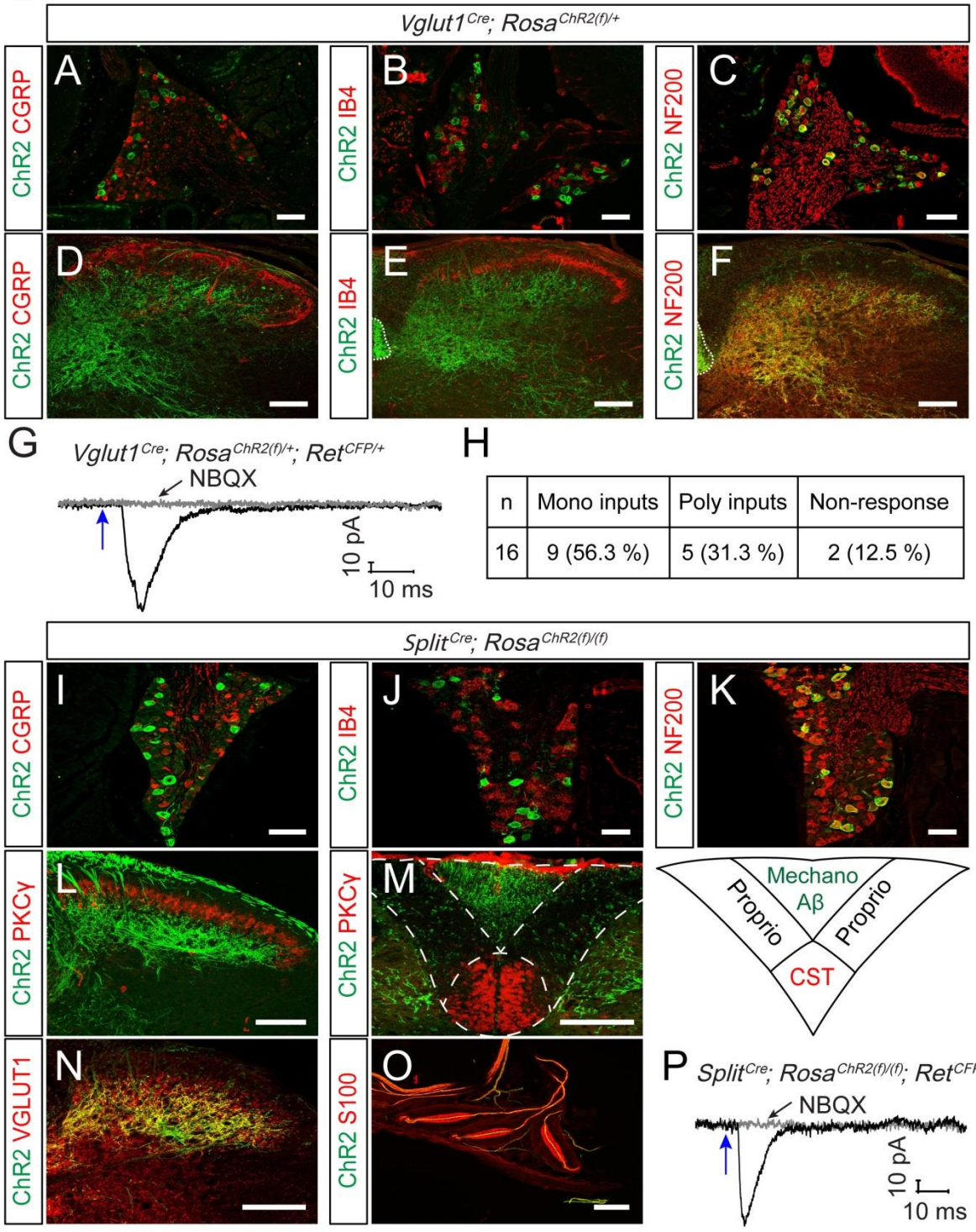


| n | Mono inputs | Poly inputs | Non-response |
|---|---|---|---|
| 16 | 9 (56.3 %) | 5 (31.3 %) | 2 (12.5 %) |

# Figure S5

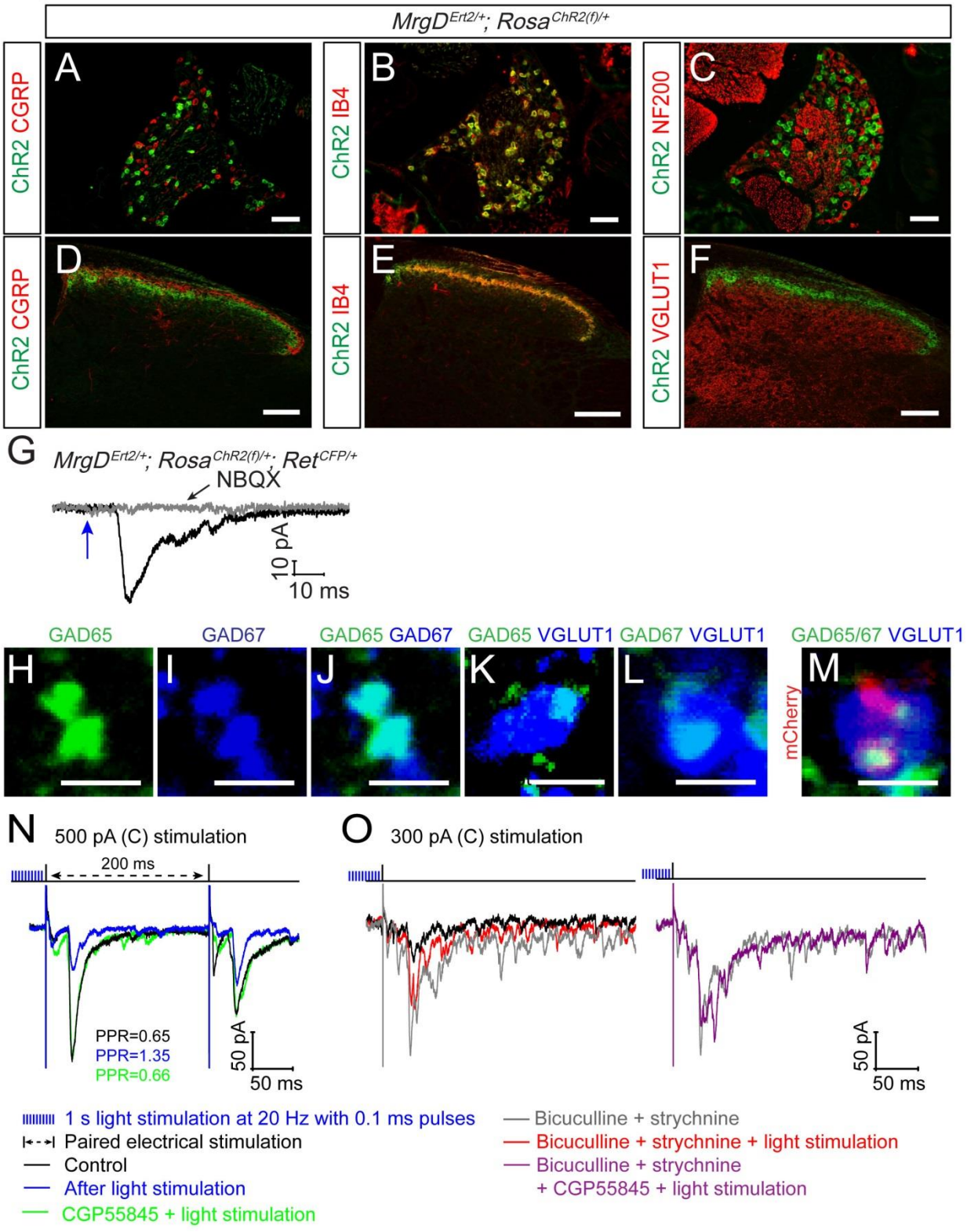
MrgD^Ert2/+; Rosa^ChR2(f)/+
ChR2 CGRP
A
ChR2 IB4
B
ChR2 NF200
C
ChR2 CGRP
D
ChR2 IB4
E
ChR2 VGLUT1
F
G
MrgD^Ert2/+; Rosa^ChR2(f)/+; Ret^CFP/+
NBQX
10 pA
10 ms
GAD65
GAD67
GAD65 GAD67
GAD65 VGLUT1
GAD67 VGLUT1
GAD65/67 VGLUT1
H
I
J
K
L
M
mCherry
N
500 pA (C) stimulation
200 ms
PPR=0.65
PPR=1.35
PPR=0.66
50 pA
50 ms
O
300 pA (C) stimulation
50 pA
50 ms
1 s light stimulation at 20 Hz with 0.1 ms pulses
Paired electrical stimulation
Control
After light stimulation
CGP55845 + light stimulation
Bicuculline + strychnine
Bicuculline + strychnine + light stimulation
Bicuculline + strychnine
+ CGP55845 + light stimulation

Figure S6

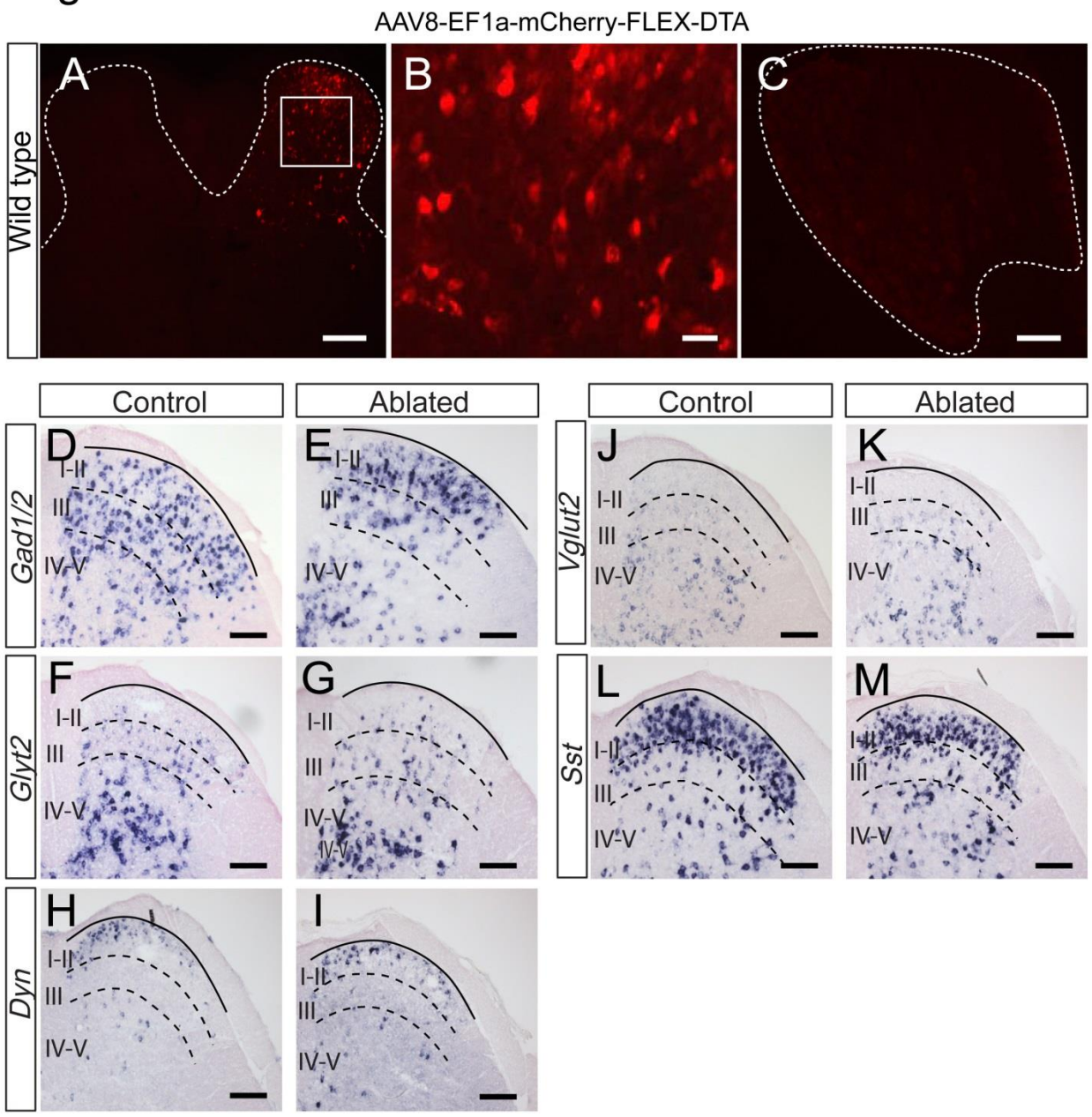
AAV8-EF1a-mCherry-FLEX-DTA
Wild type
A
B
C
Control
Ablated
Control
Ablated
Gad1/2
D
E
Vglut2
J
K
Glyt2
F
G
Sst
L
M
Dyn
H
I
I-II
III
IV-V

# Figure S7

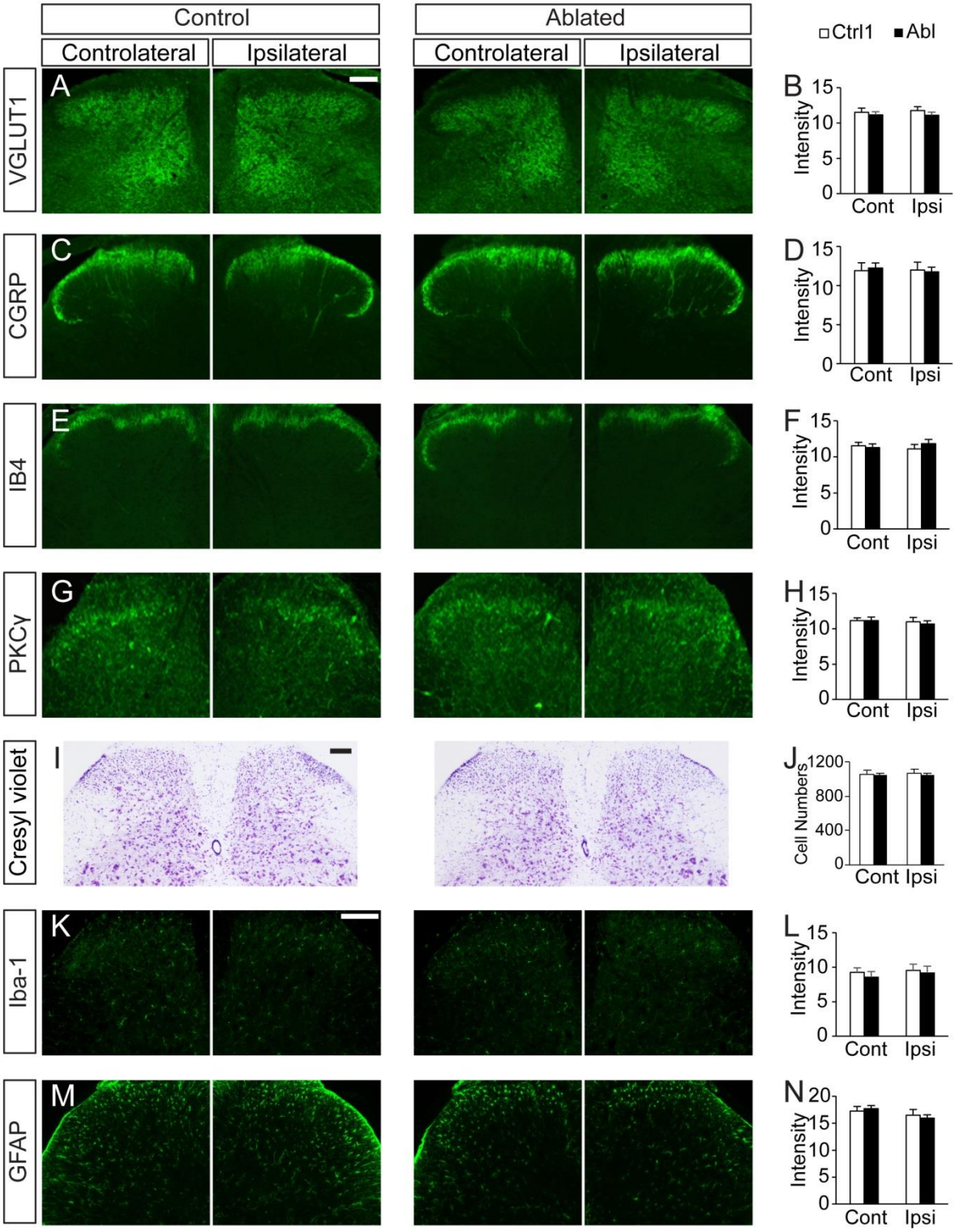
Control
Ablated
Controlateral
Ipsilateral
Controlateral
Ipsilateral
□Ctrl1 ■Abl
VGLUT1
A
B
Intensity
15
10
5
0
Cont
Ipsi
CGRP
C
D
IB4
E
F
PKCγ
G
H
Cresyl violet
I
J
Cell Numbers
1200
800
400
0
Iba-1
K
L
GFAP
M
N
20

# Figure S8

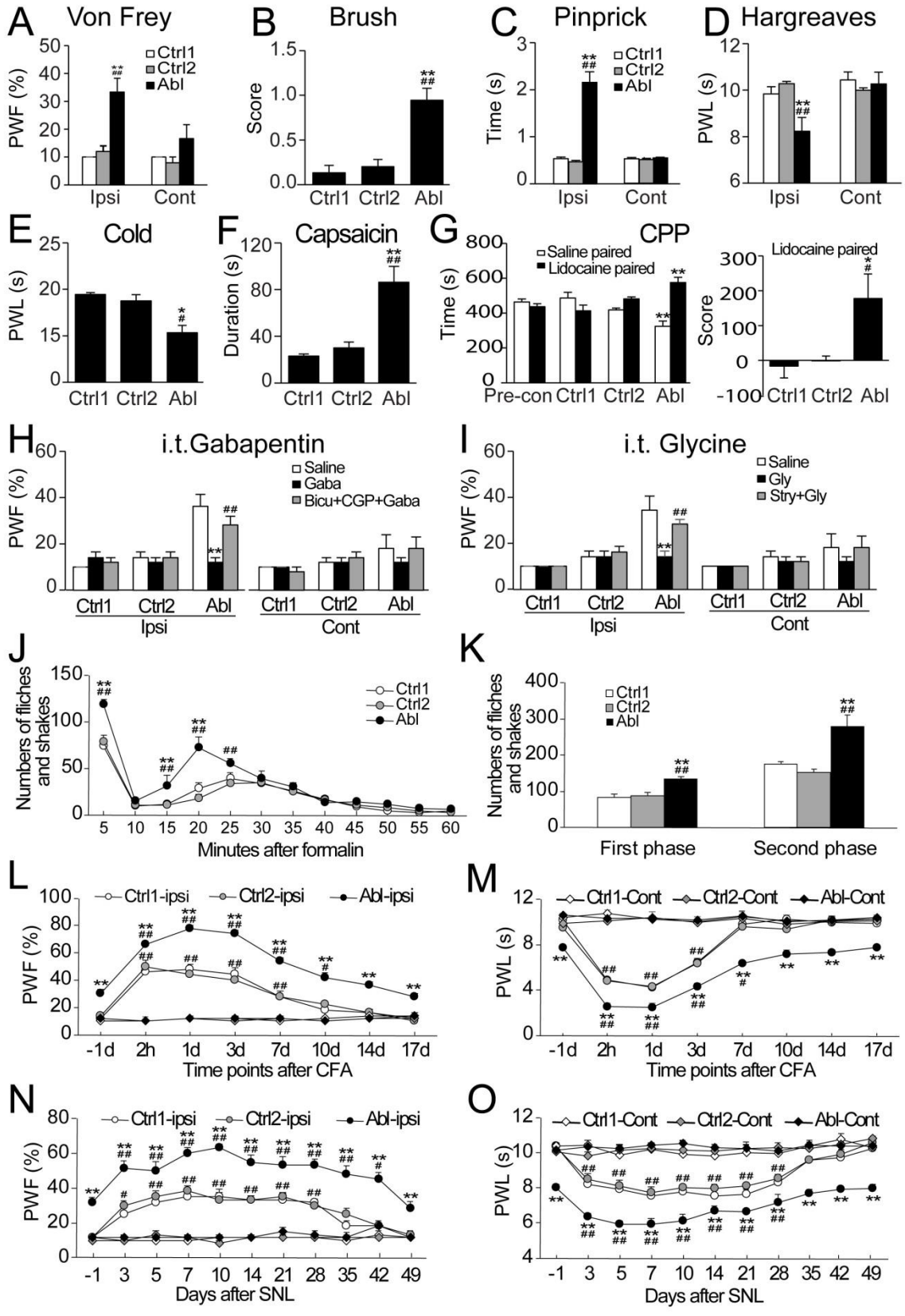
A
Von Frey
PWF (%)
Ctrl1
Ctrl2
Abl
Ipsi
Cont
B
Brush
Score
Ctrl1 Ctrl2 Abl
C
Pinprick
Time (s)
D
Hargreaves
PWL (s)
E
Cold
F
Capsaicin
Duration (s)
G
CPP
Saline paired
Lidocaine paired
Pre-con Ctrl1 Ctrl2 Abl
Lidocaine paired
H
i.t.Gabapentin
Saline
Gaba
Bicu+CGP+Gaba
I
i.t. Glycine
Gly
Stry+Gly
J
Numbers of fliches and shakes
Minutes after formalin
K
First phase
Second phase
L
Ctrl1-ipsi
Ctrl2-ipsi
Abl-ipsi
Time points after CFA
M
Ctrl1-Cont
Ctrl2-Cont
Abl-Cont
N
Days after SNL
O

## 2. Supplemental Figure Legends

**Figure S1, related to Figure 1. Expression of *Ret* mRNA in the spinal dorsal horn during postnatal development.**

(A-O) Expression of *Ret* mRNA in the spinal dorsal horn was examined in transverse sections of postnatal mouse spinal cord using *in situ* hybridization. RET+ dDH cells are found in all spinal cord levels. (A-F) From postnatal day 1 (P1) to 1 postnatal week (pw), RET+ cells are enriched in deep lamina layers (lamina III, IV and V), especially in layer III. (G-I) Around 2pw, RET+ cells are found in both the superficial and deep dorsal horn layers. (J-O) Expression of *Ret* decreases after 3pw. The dashed lines indicate the border between different layers. Scale bars, 100 μm. (P-Y) Genetic tracing of the early RET+ dDH neurons with Tdt by treating E18 $Ret^{Ert2/+}$; $Rosa^{Tdt(f)/+}$ embryos with 10 mg tamoxifen. Tdt+ neurons are located in VGLUT1+ deep DH layers (layer III through V) during postnatal development (from P1 to 5pw), suggesting that the expression of *Ret* in the superficial DH layers at 2pw and later is due to its dynamic expression but not cell migration. Scale bars, 100 μm. (Z) Quantification of the number of genetically traced early RET+ dDH neurons in the superficial (VGLUT1-) and deep (VGLUT1+) layers. 6 to 8 sections per mouse, n=3 $Ret^{Ert2/+}$; $Rosa^{Tdt(f)/+}$ mice for each stage. (AA-DD) Double *in situ* hybridization of *Ret* and transcripts of endogenous opioid-like peptides, *Dyn* and *Enkephalin* in P1 wild type mouse spinal cord sections. Scale bars, 100 μm (AA, CC) and 20 μm (BB, DD). Note that there is no overlap between RET+ and Dyn+ or Enkephalin+ neurons.

**Figure S2, related to Figure 1. Characterization of the molecular identity of early RET+ dDH neurons.**

(A-J) Double *in situ* hybridization of *Tdt* and *Ret, Vgat, Gad1/2, Glyt2* and *Vglut2* transcripts in

3pw *Ret*$^{Ert2/+}$; *Rosa*$^{Tdt(f)/+}$ mice, which were treated with tamoxifen at P7-9 for labeling early RET+ neurons with *Tdt*. Scale bars, 100 μm. Note that 61.3±2.7%, 80.9±3.9%, 47.4±2.1%, 50.7±2.4%, 11.4±1.2% of *Tdt*+ neurons are RET+, Vgat+, Gad1/2+, Glyt2+ and Vglut2+, respectively. Conversely, 56.5±7.6%, 35.8±3.5%, 28.8±2.0%, 37.1±1.1%, 5.3±0.1% of RET+, Vgat+, Gad1/2+, Glyt2+ and Vglut2+ neurons, respectively, are Tdt+. (K-V) Co-immunostaining of the spinal inhibitory neuronal markers, PV and nNOS, and the excitatory neuronal marker PKCγ with early RET+ or RET+ dDH neurons, which are labeled with Tdt or CFP in 4pw *Ret*$^{Ert2/+}$; *Rosa*$^{Tdt(f)/+}$ and *Ret*$^{CFP/+}$ mice, respectively. Scale bars, 100 μm and 20 μm. (W) Quantification of the overlap rate between genetically traced early RET+ or RET+ dDH neurons and PV in 4pw *Ret*$^{Ert2/+}$; *Rosa*$^{Tdt(f)/+}$ (23.7±3.5%) or *Ret*$^{CFP/+}$ (30.9±2.7%) mice. 6 to 8 sections per mouse, n= 3 mice for each genotype.

**Figure S3, related to Figure 2. Whole cell recording from RET+ dDH neurons in *Ret*$^{CFP/+}$ mice and generation of a dorsal horn specific *Gsx*$^{Cre}$ BAC transgenic mouse line.**

(A-B) Images showing whole cell patch clamp recording with RET+ dDH neurons in a spinal transverse slice of a 4pw *Ret*$^{CFP/+}$ mouse. Scale bars, 100 μm and 20 μm. (C-F) Recorded neurons were labeled with Alexa594-conjugated neurobiotin. After recording, spinal cord slices were stained with IB4 and anti-GFP antibodies to confirm that the recorded neurons are CFP+ and located in DH deep layer (ventral to IB4+ lamina II layer). Scale bars 100 μm (C), 10 μm (D-F). (G) Schematic showing genomic structure of the *Gsx1* gene and the recombination strategy used to generate a *Gsx*$^{Cre}$ bacterial artificial chromosome (BAC). (H-J) Recombination activities of *Gsx1*$^{Cre}$ BAC transgenic founder mice were examined by crossing to a *Tau*$^{nlacZ(f)}$ reporter line. We screened seven founder lines (data not shown) and found that founder line #6

mediates high-level recombination in the dorsal spinal cord and hindbrain, as shown here. This line was used for subsequent experiments. (H) Whole mount LacZ staining of E13.5 *Gsx1*$^{Cre}$*; Tau*$^{nlacZ(f)/+}$ embryos. Scale bars, 1 mm. N=5 mice from two litters. (I) Whole mount lacZ staining of P2 *Gsx1*$^{Cre}$*; Tau*$^{nlacZ(f)/+}$ spinal cord, which further confirms that recombination in founder line #6 is enriched in the dorsal spinal cord. D: dorsal, V: ventral. Scale bar, 1 mm. N=3 mice. (J) *In situ* hybridization of *Tdt* in a spinal cord transverse section from a P0 *Gsx1*$^{Cre}$*; Rosa*$^{Tdt(f)/+}$ mouse. *Gsx1*$^{Cre}$ recombination activity, which is indicated by *Tdt* expression, is strong in the dorsal horn but rare in in the ventral horn and DRGs (dashed line indicates DRG). Scale bar, 100 μm.

**Figure S4, related to Figure 3. Characterization of *Vglut1*$^{Cre}$*; Rosa*$^{ChR2(f)/+}$ and *Split*$^{Cre}$*; Rosa*$^{ChR2(f)/(f)}$ mice.**

(A-F) ChR2 expression in DRG neurons and their central terminals of 3pw *Vglut1*$^{Cre}$*; Rosa*$^{ChR2(f)/+}$ mice. Almost all ChR2+ neurons express NF200 but not CGRP or IB4 (A-C). In addition, ChR2+ central terminals overlap with VGLUT1+ but not CGRP+ or IB4+ terminals in the spinal cord DH. Note that ChR2 is also expressed in corticospinal tract (dashed outline) (D-F). Scale bars, 100 μm. This expression pattern indicates that ChR2 is expressed in large-diameter DRG neurons and corticospinal tract of *Vglut1*$^{Cre}$*; Rosa*$^{ChR2(f)/+}$ mice. (G) A representative trace of a light-induced EPSC (black) recorded from a RET+ dDH neuron in a spinal slice of a 2pw *Vglut1*$^{Cre}$*; Rosa*$^{ChR2(f)/+}$*; Ret*$^{CFP/+}$ mouse. This EPSC was blocked by 10 μM of an AMPA receptor antagonist, NBQX (gray trace). (H) Quantification of mono- and polysynaptic inputs onto recorded RET+ dDH neurons by light stimulation in *Vglut1*$^{Cre}$*; Rosa*$^{ChR2(f)/+}$*;Ret*$^{CFP/+}$ mice. Mono or polysynaptic $EPSC_{LS}$ were differentiated by 0.2 Hz, 20 times light stimulation. (I-O) ChR2 expression in DRG neurons and their central and peripheral

terminals of 3pw *Split*$^{Cre}$*; Rosa*$^{ChR2(f)/(f)}$ mice. Almost all ChR2+ neurons express NF200 but not CGRP or IB4 (I-K). ChR2+ central terminals are located ventral to PKCγ+ interneurons (L) and overlap with VGLUT1+ layers (N). In addition, ChR2+ fibers are found in the dorsal middle part of dorsal column where ascending axons of Aβ mechanoreceptors travel but not in the ventral region where PKCγ+ cortical spinal tract travels (M). ChR2+ peripheral terminals innervate pacinian corpuscles (O). This expression pattern suggests that ChR2 is mainly expressed in large-diameter Aβ mechanoreceptors, but not in corticospinal tract of *Split*$^{Cre}$*; Rosa*$^{ChR2(f)/(f)}$ mice. Scale bars, 100 μm. (P) A representative trace of a light-induced EPSC (black) recorded from a RET+ dDH neuron in a spinal slice of a 4pw *Split*$^{Cre}$*; Rosa*$^{ChR2(f)/(f)}$*;Ret*$^{CFP/+}$ mouse. This EPSC was blocked by 10 μM of an AMPA receptor antagonist, NBQX (gray trace).

**Figure S5, related to Figure 4 and 5. Characterization of *MrgD*$^{Ert2/+}$*; Rosa*$^{ChR2(f)/+}$ mice and presynaptic inhibition of the early RET+ dDH neurons onto primary afferent terminals through $GABA_B$ receptors**

(A-F) ChR2 expression in DRG neurons and their central terminals of 4pw *MrgD*$^{Ert2/+}$*; Rosa*$^{ChR2(f)/+}$ mice. Almost all ChR2+ neurons overlap with IB4+ but not CGRP+ or NF200+ neurons (A-C). In addition, ChR2+ central terminals overlap with IB4+ but not with CGRP+ or VGLUT1+ terminals in the spinal cord DH (D-F). This expression pattern demonstrates that ChR2 is expressed in non-peptidergic nociceptors of *MrgD*$^{Ert2/+}$*; Rosa*$^{ChR2(f)/+}$ mice. Scale bars, 100 μm. (G) A representative trace of a light induced EPSC (black) recorded from a RET+ dDH neuron in a spinal slice of a 4pw *MrgD*$^{Ert2/+}$*; Rosa*$^{ChR2(f)/+}$*;Ret*$^{CFP/+}$ mouse. This EPSC can be blocked by 10 μM NBQX (gray trace). Blue arrow indicates the light stimulation. (H-J) Co-localization of GAD65+ puncta and GAD67+ puncta in the dDH. Scale bars, 2 μm. (K and L)

Immunostaining of antibodies against VGLUT1 and GAD65 or GAD67 in spinal cord sections of 4 pw AAV1-Flex-ChR2-mCherry injected *Ret*$^{Ert2}$ mice. Note that both GAD65+ and GAD67+ puncta are in contact with VGLUT1+ puncta in the DH, suggesting that both GAD65 and GAD67 can be used as markers for DH pre-synaptic inhibition. (M) Triple staining of mCherry, antibodies against both GAD65 and GAD67, and antibody against VGLUT1 in the same mouse spinal cord sections. Note that mCherry positive neurites contain GAD+ puncta that are in close contact with VGLUT1+ puncta, suggesting that early RET+ dDH neurons may inhibit Aβ primary afferents presynaptically. Scale bars, 2 μm. (N) C specific responses of a ChR2 negative, non-light responsive (no $IPSC_L$ and $EPSC_L$) DH neuron in a dorsal root attached sagittal or transverse spinal cord slice from a 3 to 4pw *RetErt2/+;AAV8-Flex-ChR2* mouse. Light stimulation (1 second of 20 Hz light stimulation, 0.1 ms light pulses) reduced C-eEPSC amplitude and increased PPR. The light induced changes were blocked by 2 μM of the $GABA_B$ receptor antagonist, CGP 55845, suggesting that early RET+ dDH neurons execute their pre-synaptic inhibition onto C afferents through $GABA_B$ receptors. (H) Recording of a ChR2 negative, non-light responsive superficial DH neurons in a dorsal root attached sagittal or transverse spinal cord slice of a 3 to 4pw *Ret*$^{Ert2/+}$*;AAV8-Flex-ChR2* mouse. Upon pharmacological dis-inhibition (10 μM biuculline and 0.4 μM strychnine perfusion), this DH neuron displays C intensity triggered hyperactivity. This hyperactivity is significantly reduced by activation of early RET+ DH neuron using optical stimulation. 2 μM CGP 55845 pretreatment prevents the effect of early RET+ dDH neuron activation (1 second of 20 Hz light stimulation, 0.1 ms light pulses), suggesting that early RET+ dDH neurons execute this function through $GABA_B$ receptors as well.

**Figure S6, related to Figure 6. Preferential infection of DH neurons by intraspinal injection of AAV8 and the normal spinal cord laminar structure of control and DTA Abl mice.**

(A-C) Representative images of spinal cord (A-B) and ipsilateral lumbar DRG (C) sections of 9pw unilateral AAV8- Flex-DTA injected wild type mice. Scale bars: A, 100 μm; B, 20 μm; C, 50 μm. N=3 mice. Note that red fluorescent cells present in the spinal cord DH but not DRG, indicating that AAV8 preferentially infects the spinal cord DH. (D-I) *In situ* hybridization of spinal cord DH inhibitory and excitatory neuronal markers, *Gad1/2* (D-E), *Glyt2* (F-G), *Dyn* (H-I), *Vglut2* (J-K) and *Sst* (L-M), in lumbar spinal cord sections of 4pw control and DTA Abl mice. Around 18% of GAD+ DH neurons are reduced in DTA Abl mice. Note that the spinal cord laminar structure marked by different molecular markers is comparable between the two groups of mice. Sections were collected from the center of the injection site, which is indicated by the expression of red fluorescent protein. Scale bars, 100 μm, 4 to 6 sections per mice for each marker, n=3 mice.

**Figure S7, related to Figure 6. No obvious structural change, cell death, or inflammatory responses were detected in the adult mouse dorsal horn upon specific ablation of early RET+ dDH neurons.**

(A-H) Immunostaining of VGLUT1+ (A, B), CGRP+ (C, D), IB4+ afferents (E, F), or PKCγ+ excitatory neurons (G, H) in the dorsal horn of the control 1 (Ctrl1) and DTA ablated (Abl) mice. No apparent change was found between these two groups. (A, C, E, G) Representative images, scale bar, 100 μm. (B, D, F, H) Statistical summary of the contralateral and ipsilateral sides. 4 to 6 sections/mouse and n=5 mice/group. (I) Representative cresyl-violet staining images show similar laminar structure and neuronal architecture in spinal cord grey matter between Ctrl1 and

DTA Abl mice. Scale bar, 100 μm. (J) Statistical summary of the numbers of cresyl-violet stained cells in spinal cord grey matter on the ipsilateral and contralateral sides. 4 to 6 sections/mouse. Ctrl1: n=6 mice; Abl: n=9 mice. (K-N) Immunostaining of microglia marker Iba1 and astrocyte marker GFAP in the dorsal horn of Ctrl1 and DTA Abl mice. No activation of spinal cord glial cells was seen in DTA Abl mice as compared to Ctrl1. (K, M) Representative images, scale bar, 100 μm. (L, N) Statistical summary of signal intensity of Iba1 (L) and GFAP (N) immunoreactivity. 4 to 6 sections/mouse and n=6 mice/group.

**Figure S8, related to Figure 7. Pain behaviors in naïve, formalin-injected, CFA-injected, or SNL adult female mice upon specific ablation of RET+ dDH neurons.**

(A) A significant increase in paw withdrawal frequency (PWF) to static mechanical stimulation by a 0.07 g Von Frey filament on the ipsilateral (Ipsi), but not contralateral (Cont), side of DTA ablated (Abl) (n=6) was observed as compared to control group 1 (Ctrl1; n=9) or control group 2 (Ctrl2; n=5) mice. **$p < 0.01$ vs the corresponding Ctrl1 and ## $p < 0.01$ vs the corresponding Ctrl2. (B and C) Marked increases in dynamic allodynia score to a smooth paint brush (B) and in paw withdrawal duration to noxious mechanical stimulation by a safety pin (C) were observed on the ipsilateral side of DTA Abl mice (n=6/stimulation) as compared to Ctrl1 (n=5 in B; n=9 in C) or Ctrl2 (n=5/stimulation). **$p < 0.01$ vs the corresponding Ctrl1 and ## $p < 0.01$ vs the corresponding Ctrl2. (D) A profound reduction in paw withdrawal latency (PWL) to noxious heat on the ipsilateral (Ipsi), but not contralateral (Cont), side of DTA Abl (n=5) was observed as compared to Ctrl1 (n=6) or Ctrl2(n=5) mice. **$p < 0.01$ vs the corresponding Ctrl1 and ## $p < 0.01$ vs the corresponding Ctrl2. (E) A marked decrease in PWL to noxious cold (0℃) on the ipsilateral side of DTA Abl (n=5) was observed as compared to Ctrl1 (n=6) or Ctrl2 (n=5) mice.

*p < 0.05 vs the corresponding Ctrl1 and # p < 0.05 vs the corresponding Ctrl2. (F) A significant increase in the duration of paw licking/lifting within 5 min after capsaicin injection on the injected side of DTA Abl was observed as compared to Ctrl1 or Ctrl2 mice. n=5/group. **p < 0.01 vs the corresponding Ctrl1 and ## p < 0.01 vs the corresponding Ctrl2. (G) Left panel: Intrathecal lidocaine (0.04%, 5 μl) increased the time that DTA Abl mice (n=5) spent in its paired chamber, with a corresponding decrease in the saline-paired chamber. Mice from either Ctrl1 (n=6) or Ctrl2 (n=5) showed no chamber preference. **p < 0.01 vs the corresponding pre-conditioning (Pre-con) values. Right panel: Difference scores (test time - preconditioning time spent in the lidocaine chamber) confirmed that DTA Abl but not Ctrl1 and Ctrl2 mice displayed a preference for lidocaine chamber. *p < 0.05 vs the corresponding Ctrl1 and # p < 0.05 vs the corresponding Ctrl2. (H and I) The significant increase in PWF on the ipsilateral (Ipsi) side of DTA Abl mice was abolished by intrathecal administration of gabapentin (Gaba, 50 μg/5 μl) or glycine (Gly, 100 μg/5 μl). The Gaba effect was completely reversed by intrathecal co-administration of bicuculline (Bicu, 0.1 μg/5 μl) and CGP55845 (CGP, 0.1 μg/5 μl) and the Gly effect by intrathecal co-administration of strychnine (Stry, 1 μg/5 μl). None of the drugs altered basal PWLs on the contralateral (Cont) side of DTA Abl mice or on both sides of Ctrl1 or Ctrl2 mice. n=5/treatment. **p < 0.01 vs the corresponding saline-treated DTA Abl mice and ## p < 0.01 vs the corresponding Gaba- or Gly-treated DTA Abl mice. (J and K) Numbers of formalin-induced licking and shaking in both first and second phases from DTA Abl mice were greater than those from Ctrl1 or Ctrl2 mice. n=5/group. (J) Time course of formalin-induced behaviors. (K) Summary of behaviors in the first and second phases. **p < 0.01 vs the corresponding Ctrl1 and ## p < 0.01 vs the corresponding Ctrl2. (L, M) The magnitudes and durations of CFA-induced static mechanical allodynia (L) and thermal hyperalgesia (M) in DTA Abl mice were

greater than those in either Ctrl1 or Ctrl2 mice. n=5/group. **$p < 0.01$ vs the corresponding time points in the Ctrl1 and # $p < 0.05$ or ## $p < 0.01$ vs the corresponding baseline (-1d) on the ipsilateral side. (N and O) The magnitudes and durations of SNL-induced static mechanical allodynia (N) and thermal hyperalgesia (O) in the DTA Abl mice were greater than those in either Ctrl1 or Ctrl2 mice. n=6/group. **$p < 0.01$ vs the corresponding time points in the Ctrl1 and #$p < 0.05$ or ##$p < 0.01$ vs the corresponding baseline (-1d) on the ipsilateral side.

## 3. Supplemental Tables

**Table S1, related to Figure 6 and 7. Genotypes and virus injection in control and ablation groups for behavior tests.**

| Groups | Genotype | Virus |
|---|---|---|
| Control 1 | WT | AAV8-EF1α-mCherry-FLEX-DTA |
| Control 2 | *Ret*$^{Ert2}$ | AAV8-CMV-TurboRFP-WPRE-rBG |
| Ablated | *Ret*$^{Ert2}$ | AAV8-EF1α-mCherry-FLEX-DTA |

**Table S2, related to Figure 7. Mean (SEM) Changes in locomotor tests.**

| Male | Control 1 | Control 2 | Ablated | Female | Control 1 | Control 2 | Ablated |
|---|---|---|---|---|---|---|---|
| Placing | 5 (0) | 5 (0) | 5 (0) | Placing | 5 (0) | 5 (0) | 5 (0) |
| Grasping | 5 (0) | 5 (0) | 5 (0) | Grasping | 5 (0) | 5 (0) | 5 (0) |
| Righting | 5 (0) | 5 (0) | 5 (0) | Righting | 5 (0) | 5 (0) | 5 (0) |

n=18/group. 5 trials.

**Table S3, related to Figure 8. Genotypes, virus injection, and treatment in control and activation groups for behavior tests.**

| Groups | Genotype | Virus | Treatment | Anticipated outcome |
|---|---|---|---|---|
| Ctrl-Veh | WT | AAV8-hSyn-DiO-hM3Dq-mCherry | Vehicle | None |
| hM3Dq-Veh | *Ret*$^{Ert2}$ | AAV8-hSyn-DiO-hM3Dq-mCherry | Vehicle | None |
| Ctrl-CNO | WT | AAV8-hSyn-DiO-hM3Dq-mCherry | CNO | None |
| hM3Dq-CNO | *Ret*$^{Ert2}$ | AAV8-hSyn-DiO-hM3Dq-mCherry | CNO | Activate RET+ dDH neurons |

## 4. Supplemental Experimental Procedures

### Mouse lines and tamoxifen treatments

*Ret*$^{Ert2}$, *Ret*$^{CFP(f)}$, *Ret*$^{CFP}$, *Tau*$^{nLacZ(f)}$ and *Rosa*$^{Tdt(f)}$ mouse lines were described previously (Luo et al., 2009; Madisen et al., 2010; Uesaka et al., 2008). The *Split*$^{Cre}$ mice mouse line (Rutlin et al., 2014) was imported from Dr. David Ginty's lab at the Harvard University, which was originally generated by the Gensat project. The *Vgat*$^{Cre}$ mouse line (Vong et al., 2011) was provided by Dr. Zhaolan Zhou at the University of Pennsylvania, which was purchased from the Jackson Lab. The *Vglut1*$^{Cre}$ and *Rosa*$^{ChR2(f)}$ mouse lines (Harris et al., 2014; Madisen et al., 2012) were also obtained from the Jackson Lab. The *MrgD*$^{Ert2}$ mouse line was generated by the Luo lab, details of which will be published in an upcoming paper. The *Ret*$^{Ert2}$ and *Rosa*$^{Tdt(f)}$ mouse lines were mated daily and plugs were checked each morning. The time when a mouse was found to have plug was considered as E0.5. Pregnant females were oral gavaged to specifically label the early RET+ dDH neurons with 10 mg of tamoxifen (in sunflower seed oil, oral gavage) at E18. *MrgD*$^{Ert2/+}$; *Rosa*$^{ChR2(f)/+}$ pups were treated with 0.5 mg of tamoxifen (in sunflower seed oil, I.P. injection) per day for three days from P14 to P16. For *Ret*$^{Ert2}$ pups with intra-spinal injection of viruses, we usually conducted tamoxifen treatment (I.P. injection, 0.3 mg per day) between P7-P9 (the virus injection was conducted at P6). For sparse labeling, we treated for one day with 0.1 mg at P7.

### Maintenance of mice used for behavior assays

Adult male or female mice with desired genotypes weighing 20–30 g were kept in a standard 12-h light/dark cycle, with water and food pellets available *ad libitum*. All procedures used were approved by the Animal Care and Use Committee at Rutgers New Jersey Medical School, and consistent with the ethical guidelines of the National Institutes of Health and the International

Association for the Study of Pain. All efforts were made to minimize animal suffering and to reduce the number of animals used. All of the experimenters were blind to treatment condition.

**Generation of *Gsx1$^{Cre}$* mice**

To generate *Gsx1$^{Cre}$* mice, we used BAC BX1725 (RP24-352K2), which is the same BAC used by GENSAT and drives dSC specific expression of GFP at E15.5. We ordered BAC from Children's Hospital Oakland Research Institute and used a bacteria recombination system (Copeland et al., 2001) to insert a FLAG tagged Cre cassette into the first encoding exon of *Gsx1* gene. The recombined BAC DNA was injected to the nucleus of fertilized eggs by the transgenic core of the University of Pennsylvania. More than 10 founder lines were generated and 7 of them were screened for their recombination pattern by crossing to a reporter line, *Tau$^{nlacZ(f)}$* (Hippenmeyer et al., 2005).

***In situ* hybridization**

All cRNA probes used in this study (*Ret, Gad1/2, Glyt2, Sst, Prodynorphin, Vglut2, Preproenkephalin*, and *Vgat*) have been described elsewhere ((Luo et al., 2009) and the Allen Brain Atlas) and were conjugated with either digoxigenin (DIG) or fluorescein isothiocyanate (FITC) (Roche). For tissue preparation to perform RNA *in situ* hybridization, the intact spinal columns were dissected from CO2 euthanized mice and rapidly frozen in OCT on a dry-ice/ethanol bath. 20 μm cryosections were collected on Superfrost Plus slides (Fisher, 22-034-979) and allowed to dry for at least 2 hours at room temperature. All steps prior to hybridization were carried out under RNase free conditions. *In situ* hybridization and double fluorescent in-situ hybridization (FISH) were performed as previously described (Fleming et al., 2012).

For ISH combined with immunostaining, the normal hybridization procedure was followed, using DIG-labeled riboprobe and BCIP/NBT color reaction. Upon development of appropriate signal, the sections were post-fixed with 4% paraformaldehyde (PFA), followed by blocking in 5% lamb serum in 0.2% Triton X-100 phosphate buffer (PBT). Normal immunohistochemistry was performed with anti-GFP or anti-dsRED primary antibodies (1:500) overnight (ON), followed by a second day of 3X 10 minute PBT washes and 1 hour of appropriate secondary antibody at 1:500. BCIP/NBT images were pseudo-colored in Photoshop. This procedure works when GFP or dsRED is membrane tethered, such as fused to ChR2.

**Immunohistochemistry**

Ketamine/xylazine/acepromazine cocktail anesthetized mice were transcardially perfused with 4% PFA in phosphate buffer solution (PBS). Intact lumbar spinal columns were dissected and post-fixed for 2-4 hours in 4% PFA in PBS at 4°C, cryoprotected in 30% sucrose in PBS O/N at 4°C, and embedded in OCT. 20 μm cryosections of spinal cord or DRG were collected on Superfrost Plus slides, and allowed to dry at room temperature for at least two hours. Sections were washed in PBT (3X 10 minutes), and then blocked in PBS containing 5% lamb serum and 0.2% TritonX-100 for 1 hour at room temperature. Primary antibodies were diluted in the same buffer, and incubated O/N at 4°C, then washed in PBT (3X 10 minutes). Secondary antibodies were incubated in blocking buffer at 1:500 dilution for one hour at room temperature. Slides were then washed in PBT (3X 10 minutes) and mounted with Fluormount. Images were collected using a Leica SP5 confocal microscope, Leica DM5000B microscope, or a Nikon TE2000E fluorescence microscope. Primary antibodies used include chicken anti-GFP (1:1,000;

Aves, GFP-1020), rabbit anti-GFP (1:1,000, Invitrogen, A-11122), mouse anti-NeuN (1:1,000, Millipore, MAB377), rabbit anti-CGRP (1:5,000; Immunostar, 24112), mouse anti-PKCγ (1:50, Invitrogen, 13-3800), rabbit anti-NF200 (1:2,000; Sigma, N4142), Guinea pig anti-VGluT1 (1:1,000, Millipore, AB5905) rabbit anti-PV (1:1,000, Swant, PV25), rabbit anti-nNOS (1:1,000, Immunostar, 24431), Alexa 488 or 594 conjugated IB4 (1:200; Invitrogen, I21411), rabbit anti-dsRED (1:1,000, Clontech, 632496), guinea pig anti-VGLUT2 (1:1,000, Millipore, AB2251), mouse anti-GAD65 (1:100, Developmental Studies Hybridoma Bank at the University of Iowa, AB 528624), mouse anti-GAD67 (1:1,000, Millipore, MAB5406), rabbit anti-GAD65 (1:1,000, a gift from Jessell lab), rabbit anti-Iba-1 (1:1,000, WAKO, 019-19741), and mouse anti-GFAP (1:500, cell signaling, 3670). Secondary antibodies are Alexa 488, Alexa 594, or Alexa 647 conjugated goat anti-rabbit antibody, Alexa 488 conjugated goat anti-mouse antibody, Alexa 488 conjugated goat anti-chicken antibody, and Alexa 488 conjugated goat anti-guinea pig antibody. Secondary antibodies were purchased from Invitrogen or Jackson Immunoresearch.

**Intraspinal AAV virus injections**

Spinal cord microinjection of P6 mice was carried out as previously described with minor modifications (Inquimbert et al., 2013). Briefly, under constant anesthesia (~3% of isoflurane), a midline incision was made at the caudal end of the rib cage and the vertebra L1 was exposed and removed with small forceps. After the spinal cord was exposed, the mouse was placed in a stereotaxic frame and the vertebral column was immobilized. A glass micropipette (tip diameter 20-40 μm) was positioned 200 μm lateral from the posterior median sulcus and 200 μm below the dorsal surface of the spinal cord at the level of L4 spinal cord. A micropipette was connected

to a 5 µl Hamilton syringe and an Ultra Micro Pump III (UMP3) with a SYS-micro4 controller attachment (World Precision, Sarasota, USA) was used to inject viral vectors at a speed 10 to 20 nl/min. 0.2 to 1 µl of viral or PBS solution was slowly injected. The micropipette was removed 10 to 15 min after injection, the surgical field was irrigated with sterile saline, and the skin incision was sutured. After recovery from anesthesia, 0.1 mg/kg buprenorphine was injected subcutaneously to alleviate pain. 2-3 weeks post-surgery, mice were sacrificed and used for physiology experiments. For behavior studies, mice were tested when they were at least 6 weeks old. For activating early RET+ dDH neurons in spinal cord slices, AAV1-CBA-Flex-ChR2(H134R)-mCherry-WPRE-SV40 ($7.86 \times 10^9$ viral units/µl) (Atasoy et al., 2008), AAV1-EF1a-DIO-hChR2(H134R)-eYFP-WPRE-hGH (AAV-Flex-ChR2-XFP) ($2.99 \times 10^{10}$ viral units/µl), or AAV8-CBA-Flex-ChR2(H134R)-mCherry-WPRE-SV40 ($7.04 \times 10^9$ viral units/µl) were used. For sparse labeling to study the morphologies of early RET+ dDH neurons, $1 \times 10^7$ viral units of AAV-Flex-ChR2-XFP virus was injected. For ablating early RET+ dDH neurons, AAV8-EF1α-mCherry-Flex-DTA ($3.3 \times 10^9$ viral units/µl) (Wu et al., 2014) was used. AAV8-CMV-TurboRFP-WPRE-rBG ($2.94 \times 10^{10}$ viral units /µl) was injected as control. For acutely activating early RET+ dDH neurons, AAV8-hSyn-DIO-hM3D(Gq)-mCherry ($7.9 \times 10^{12}$ viral units/µl) was injected. AAV8-Flex-DTA virus was initially provided by Dr. Naoshige Uchida at Harvard University and later purchased from the University of North Carolina (UNC) vector core (Chapel Hill, NC). AAV8-hSyn-DIO-hM3D(Gq)-mCherry was purchased from the UNC vector core. All other viral vectors were purchased from the University of Pennsylvania vector core (Philadelphia, PA).

**Electrophysiology**

3-5pw mice were anesthetized with a ketamine/xylazine/acepromazine cocktail. Laminectomy was performed, and the spinal cord lumbar segments were removed and placed in ice-cold incubation solution consisting of (in mM) 95 NaCl, 1.8 KCl, 1.2 $KH_2PO_4$, 0.5 $CaCl_2$, 7 $MgSO_4$, 26 $NaHCO_3$, 15 glucose, and 50 sucrose, and oxygenated with 95% $O_2$ and 5% $CO_2$, at a pH of 7.35–7.45 and an osmolality of 310–320 mOsm. Sagittal or transverse spinal cord slices (500–600 μm thick) of the attached L4 or L5 dorsal roots were prepared using a VT1200S vibratome (Leica Microsystems, Nussloch, Germany) and incubated in 34°C incubation solution for 30 min.

The slice was transferred to the recording chamber and continuously perfused with recording solution at a rate of 3–4 ml/min. The recording solution consisted of (in mM) 127 NaCl, 1.8 KCl, 1.2 $KH_2PO_4$, 2.4 $CaCl_2$, 1.3 $MgSO_4$, 26 $NaHCO_3$, and 15 glucose, oxygenated with 95% $O_2$ and 5% $CO_2$, at a pH of 7.35–7.45 and an osmolality of 300–310 mOsm. Recordings were performed at RT. Spinal cord slices were visualized with an Olympus BX 61WI microscope (Olympus Optical, Tokyo, Japan), and the substantia gelatinosa (lamina II), which is a translucent band across the dorsal horn, was used as a landmark (Figure S3A). Fluorescently labeled neurons in dorsal horn were identified by epifluorescence and recorded in the whole cell patch-clamp configuration. Glass pipettes (3–5MΩ) were filled with internal solution consisting of (in mM) 120 K-gluconate, 10 KCl, 2 MgATP, 0.5 NaGTP, 20 HEPES, 0.5 EGTA, and 10 phosphocreatine di(tris) salt at a pH of 7.29 and an osmolality of 300mOsm. In some experiments, 0.5% neurobiotin (Vector laboratories, SP-1120) was added into the internal solution to label the recorded cell. All data were acquired using an EPC-9 patch-clamp amplifier and Pulse software (HEKA, Freiburg, Germany). Liquid junction potentials were not corrected.

Firing patterns were defined as previously described (Heinke et al., 2004). The series resistance was between 10 and 25MΩ, and we discarded any experiments in which these values changed >20% during the recordings.

To evoke synaptic currents, we applied 0.1ms stimuli to the dorsal root through a suction electrode with a constant current stimulator (A365; WPI) at 0.05Hz, 0.1ms duration. We defined evoked excitatory postsynaptic currents (EPSCs) based on the threshold of stimulation intensity as previously reported: Aβ-eEPSC: 8-26pA, Aδ-eEPSC: 25-82pA; and C fibers >180pA (Nakatsuka et al., 2000; Torsney and MacDermott, 2006). We also calculated the conduction velocity (CV) based on temporal delays and dorsal root lengths to distinguish different types of afferent inputs: mean CV of Aα/β-fibers: 18.2±1.7 (13.0–25.0) meters per second; mean CV of Aδ-fibers: 5.8±0.9 (3.0–11.0) meters per second; and mean CV of C-fibers: 0.6±0.1 (0.5–0.8) meters per second. In addition, we defined these eEPSCs as monosynaptic or polysynaptic according the following criteria: for Aβ-eEPSCs and Aδ-eEPSCs, stable latency and an absence of synaptic failure during 20Hz and 10Hz stimuli, respectively, indicated a monosynaptic response. Otherwise, it was considered a polysynaptic response. For C-eEPSCs, a lack of synaptic failures during 1 Hz stimuli indicated a monosynaptic response. Otherwise it was considered polysynaptic. The paired pulse ratio (PPR) was calculated as the ratio of the second synaptic responses to the first one upon a paired-pulse stimulation. To examine CNO response of mCherry positive and mCherry negative neurons in spinal cord slices of $Ret^{Ert2}$ mice injected with AAV8-hSyn-DIO-hM3D(Gq)-mCherry, 3mM CNO was puff applied using a pressure system (10~15Psi, 100~200ms) with 2μm diameter glass pipette. Bicuculline (10μM), strychnine (0.4μM), NBQX (10μM) and TTX (1μM) were added into the recording solution for some

experiments.

**Neurobiotin labeling**

After a minimum of 15 min in the whole-cell patch-clamp configuration, a 0.5% neurobiotin filled electrode was withdrawn from the targeted neuron and the slice was immediately immersed in 4% PFA and incubated at 4°C overnight. The slice was then rinsed in PBS and treated with PBS containing 0.3% $H_2O_2$ for 60 min. After rinsing in PBS, the slice was incubated in 0.3% PBT for 10 min, followed by PBT containing Alexa-594 conjugated streptavidin (1:1000, life technologies, S-11227) for 60 min. Then, the slice was rinsed in PBT, and incubated in IB4 solution (5% of lamb serum in PBT) for overnight at 4°C. The slice was then rinsed and mounted for imaging.

**Optogenetic experiments**

Optogenetic experiments were conducted with spinal cord sagittal or transverse slices from 3-4pw *Vglut1*$^{Cre}$; *Rosa*$^{ChR2\text{-}EYFP(f)/+}$; *Ret*$^{CFP/+}$mice, *Splite*$^{Cre}$; *Rosa*$^{ChR2\text{-}EYFP(f)/(f)}$; *Ret*$^{CFP/+}$mice, *MrgD*$^{Ert2/+}$; *Rosa*$^{ChR2(f)/+;}$ *Ret*$^{CFP/+}$mice and AAV-Flex-ChR2-XFP injected *Ret*$^{Ert2}$ mice. Blue light (473 nm laser illumination (10 mW, 0.1-1 ms, Blue Sky Research, Milpitas, USA)) was delivered through a 40X water-immersion microscope objective. Light induced EPSCs ($EPSC_{LS}$) were first elicited at a frequency of 0.033 Hz (2 times/min). Mono- or polysynaptic $EPSC_{LS}$ were further differentiated by 0.2 Hz, 20 times light stimulation. We classified a connection as monosynaptic if the EPSC jitter (average standard deviation of the light-induced $EPSC_{LS}$ latency from stimulation) was < 1.6 ms (Doyle and Andresen, 2001; Wang and Zylka, 2009). To examine the effect of early RET+ neuron activity on synaptic transmission from primary afferents to

superficial DH neurons, recordings were done in superficial DH neurons of *Ret$^{Ert2}$; AAV8-Flex-ChR2-XFP* mice and high frequency light stimuli (1 second, 20 to 50 Hz, 0.1 ms light pulses) were applied to achieve strong activation of early RET+ neurons.

**Single-Cell Reverse Transcription-Polymerase Chain Reaction (single-cell RT-PCR)**

After recording, cytosol of recorded cells were suck out and gently put into an 8-well PCR reaction tube containing RT mix (1 µl RNaseOUT, 1.5 µl dNTPs and 1.5 µl oligo(dT)$_{20}$). Complementary DNA (cDNA) was synthesized using the SuperScript First-Strand Synthesis system (Invitrogen, 11904018). PCR was performed on cDNA with primers for *Pkcγ* (5'-TTTCTTCAAGCAGCCAACCTTC-3' and 5'-ATTTCCAGTTGCAGACGTCCAC-3', PCR product length=372), *Sst* (5'-AGACTCCGTCAGTTTCTGCAG -3' and 5'-CTAACAGGATGTGAATGTCTTC-3', PCR product length=264), *Prodynorphin* (5'-TGATGCCCTCTAATGTTATG -3' and 5'-ATTCTTTTCCGTTGCCAAAG-3', PCR product length=360), and *Gapdh* (5'-GGTGAAGGTCGGTGTGAACG-3' and 5'-CTCGCTCCTGGAAGATGGTG-3', PCR product length=233).

**Pain Behavior Assays**

Static mechanical allodynia was measured through the paw withdrawal response to one calibrated von Frey filament (Stoelting Co., Wood Dale, IL. USA) as previously described (Tao et al., 2003; Wang et al., 2011). Briefly, each mouse was placed in a Plexiglas chamber on an elevated mesh screen. The 0.07 g von Frey filament was applied to the hind paw for approximately 1 sec and each stimulation was repeated ten times to both hind paws. The occurrence of paw withdrawal in each of these ten trials was expressed as a percent response

frequency [(number of paw withdrawals / 10 trials) X 100 = % response frequency], and this percentage was used as an indication of the amount of paw withdrawal.

Dynamic mechanical allodynia was tested through the paw withdrawal response to a smooth paint brush and calculated by using the allodynia scoring system as previously described (Duan et al., 2014). Briefly, mice were placed on an elevated wire grid and habituated for 15 min on the day of the experiment. The plantar hind paw was stimulated by light stroking with a paintbrush in the heel-to-toe direction. The test was repeated three times at intervals of at least 3 min to obtain the average score for each mouse. Dynamic allodynia was scored as follows: 0 for walking away or a very brief paw lifting, 1 for sustained lifting (>2 s) of the stimulated paw, 2 for lifting and flinching of the affected paw, and 3 for licking of the affected paw.

Mechanical hyperalgesia was examined through the paw withdrawal response to a safety pin (Cao et al., 2010). Briefly, each mouse was placed in a Plexiglas chamber on an elevated mesh screen. The tip of the pin was applied to the plantar surface of the hind paw without skin penetration. The length of time between the foot lift and the placement of the hind paw on the screen was defined as the paw withdrawal duration. Each trial was repeated 3 times at 10 min intervals.

Thermal hyperalgesia was measured by using the Hargreaves test (Tao et al., 2003; Wang et al., 2011). Briefly, each mouse was placed in a Plexiglas chamber on a glass plate under which a light box was located. Radiant heat from a Model 336 Analgesic Meter (IITC Inc./Life Science Instruments, Woodland Hills, CA. USA) was applied by aiming a beam of light through

a hole in the light box through the glass plate to the middle of the plantar surface of each hind paw. When the animal lifted its foot, the light beam was turned off. The length of time between the start of the light beam and the foot lift was defined as the paw withdrawal latency. Each trial was repeated five times at 5 minute intervals for each side. A cut-off time of 20 s was used to avoid tissue damage to the hind paw.

Cold hyperalgesia was tested though the paw withdrawal response to a cold plate, the temperature of which was monitored continuously (Li et al., 2015; Zhao et al., 2013). Briefly, a differential thermocouple thermometer (Harvard Apparatus, South Natick, MA) attached to the plate provided a temperature precision of 0.1°C. Each mouse was placed in a Plexiglas chamber on the cold plate, which was set at 0°C. The length of time between the placement of the hind paw on the plate and the animal jumping, with or without paw licking and flinching, was defined as the paw withdrawal latency. Each trial was repeated three times at 10 minute intervals for the paw on the ipsilateral side. A cutoff time of 20 s was used to avoid paw tissue damage.

Capsaicin-induced nocifensive response was examined as described previously (Fan et al., 2014). Briefly, 10 μl of vehicle (70% alcohol) or capsaicin (1 μg) was injected intradermally under the dorsal surface of the hind paw. The duration of time that the mouse spent licking and/or lifting the injected paw was measured with a stopwatch and was considered as an indicator of the nocifensive response. The mouse was observed for 5 min immediately after the injection.

The formalin test was performed as described previously (Liaw et al., 2008). Briefly, the mouse received a 10 μl intraplantar injection of 0.8% formalin. After the injection, the number of flinches and shakes was recorded in 5 minute periods for 60 minutes. We defined the first phase response as the total number of flinches and shakes during the first 10 minutes and the second phase response as the total number of flinches and shakes that occurred 10-60 minutes after the injection.

The conditioned place preference (CPP) test was carried out as described (He et al., 2012; King et al., 2009). Briefly, a CPP apparatus consists of 2 chambers separated by manual doors. Movement of mice and time spent in each chamber were monitored by photobeam arrays and automatically recorded in CPP software. Preconditioning was performed across 3 days for 30 minutes each day when mice were exposed to the environment with full access to all chambers. On day 3, a preconditioning bias test was performed to determine whether a preexisting chamber bias existed. In this test, mice were allowed to explore open field with access to all chambers for 15 minutes. Data were collected and analyzed for the duration spent in each chamber. Animals spending more than 80% or less than 20% of the total time in an end chamber were eliminated (10% of total animals) from further testing. After the precondition test, the conditioning protocol was performed as follows. The mice first received intrathecal injection with saline (5 μl) paired with a randomly chosen chamber for 30 min (without access to another chamber) in the morning, and 4 hours later, 0.04% lidocaine (5 μl) was paired with another chamber for 30 min in the afternoon. On the second day, mice were again conditioned by saline or lidocaine paired with the corresponding chamber, but the lidocaine was given in the morning and saline in the afternoon.

On the third (test) day, the mice were allowed free access to either chamber. The movement and duration each mouse spent in each chamber were recorded for 15 min. Difference scores were calculated as test time-preconditioning time spent in the lidocaine chamber.

Locomotor function was examined according to methods described previously (Atianjoh et al., 2010; Chu et al., 2005; Liaw et al., 2008). The following tests were performed for each mouse before other tests: (1) Placing reflex: The mouse was held with the hind limbs slightly lower than the forelimbs, and the dorsal surfaces of the hind paws were brought into contact with the edge of a table. The experimenter recorded whether the hind paws were placed on the table surface reflexively; (2) Grasping reflex: The mouse was placed on a wire grid and the experimenter recorded whether the hind paws grasped the wire on contact; (3) Righting reflex: The mouse was placed on its back on a flat surface and the experimenter noted whether it immediately assumed the normal upright position. Scores for placing, grasping, and righting reflexes were based on counts of each normal reflex exhibited in 5 trials.

**Pain models**

The formalin-induced inflammatory pain model, the Complete Freund's adjuvant (CFA)-induced chronic inflammatory pain model, and the fourth spinal nerve ligation (SNL)-induced neuropathic pain model were carried out as described previously (Atianjoh et al., 2010; Chu et al., 2005; Liaw et al., 2008). Saline injection or sham surgery was used as a control.

Some adult male $Ret^{Ert2}$ and control mice unilaterally injected with AAV8-hSyn-DIO-hM3D(Gq)-mCherry were subjected to the ipsilateral CFA injection or SNL surgery. On days 1

and 3 post-CFA or on days 7 and 14 post-SNL, the mice were injected i.p. with 5 mg/kg clozapine N-oxide (CNO, Sigma) or vehicle (10% DMSO in saline). Behavioral tests were carried out 1 day prior to CFA or SNL (baseline), before CNO/vehicle injection, and 1 h after CNO/vehicle injection.

## 5. Supplemental References


Atasoy, D., Aponte, Y., Su, H.H., and Sternson, S.M. (2008). A FLEX switch targets Channelrhodopsin-2 to multiple cell types for imaging and long-range circuit mapping. J Neurosci *28*, 7025-7030.

Atianjoh, F.E., Yaster, M., Zhao, X., Takamiya, K., Xia, J., Gauda, E.B., Huganir, R.L., and Tao, Y.X. (2010). Spinal cord protein interacting with C kinase 1 is required for the maintenance of complete Freund's adjuvant-induced inflammatory pain but not for incision-induced post-operative pain. Pain *151*, 226-234.

Cao, X.H., Byun, H.S., Chen, S.R., Cai, Y.Q., and Pan, H.L. (2010). Reduction in voltage-gated K+ channel activity in primary sensory neurons in painful diabetic neuropathy: role of brain-derived neurotrophic factor. J Neurochem *114*, 1460-1475.

Chu, Y.C., Guan, Y., Skinner, J., Raja, S.N., Johns, R.A., and Tao, Y.X. (2005). Effect of genetic knockout or pharmacologic inhibition of neuronal nitric oxide synthase on complete Freund's adjuvant-induced persistent pain. Pain *119*, 113-123.

Copeland, N.G., Jenkins, N.A., and Court, D.L. (2001). Recombineering: a powerful new tool for mouse functional genomics. Nat Rev Genet *2*, 769-779.

Doyle, M.W., and Andresen, M.C. (2001). Reliability of monosynaptic sensory transmission in brain stem neurons in vitro. J Neurophysiol *85*, 2213-2223.

Duan, B., Cheng, L., Bourane, S., Britz, O., Padilla, C., Garcia-Campmany, L., Krashes, M., Knowlton, W., Velasquez, T., Ren, X*., et al.* (2014). Identification of spinal circuits transmitting and gating mechanical pain. Cell *159*, 1417-1432.

Fan, L., Guan, X., Wang, W., Zhao, J.Y., Zhang, H., Tiwari, V., Hoffman, P.N., Li, M., and Tao, Y.X. (2014). Impaired neuropathic pain and preserved acute pain in rats overexpressing voltage-gated potassium channel subunit Kv1.2 in primary afferent neurons. Mol Pain *10*, 8.

Fleming, M.S., Ramos, D., Han, S.B., Zhao, J., Son, Y.J., and Luo, W. (2012). The majority of dorsal spinal cord gastrin releasing peptide is synthesized locally whereas neuromedin B is highly expressed in pain- and itch-sensing somatosensory neurons. Mol Pain *8*, 52.

Harris, J.A., Hirokawa, K.E., Sorensen, S.A., Gu, H., Mills, M., Ng, L.L., Bohn, P., Mortrud, M., Ouellette, B., Kidney, J*., et al.* (2014). Anatomical characterization of Cre driver mice for neural circuit mapping and manipulation. Front Neural Circuits *8*, 76.

He, Y., Tian, X., Hu, X., Porreca, F., and Wang, Z.J. (2012). Negative reinforcement reveals non-evoked ongoing pain in mice with tissue or nerve injury. J Pain *13*, 598-607.

Heinke, B., Ruscheweyh, R., Forsthuber, L., Wunderbaldinger, G., and Sandkuhler, J. (2004). Physiological, neurochemical and morphological properties of a subgroup of GABAergic spinal lamina II neurones identified by expression of green fluorescent protein in mice. J Physiol *560*, 249-266.

Hippenmeyer, S., Vrieseling, E., Sigrist, M., Portmann, T., Laengle, C., Ladle, D.R., and Arber, S. (2005). A developmental switch in the response of DRG neurons to ETS transcription factor signaling. PLoS Biol *3*, e159.

Inquimbert, P., Moll, M., Kohno, T., and Scholz, J. (2013). Stereotaxic injection of a viral vector for conditional gene manipulation in the mouse spinal cord. J Vis Exp, e50313.

King, T., Vera-Portocarrero, L., Gutierrez, T., Vanderah, T.W., Dussor, G., Lai, J., Fields, H.L., and Porreca, F. (2009). Unmasking the tonic-aversive state in neuropathic pain. Nat Neurosci *12*, 1364-1366.

Li, Z., Gu, X., Sun, L., Wu, S., Liang, L., Cao, J., Lutz, B.M., Bekker, A., Zhang, W., and Tao, Y.X. (2015). Dorsal root ganglion myeloid zinc finger protein 1 contributes to neuropathic pain

after peripheral nerve trauma. Pain *156*, 711-721.
Liaw, W.J., Zhu, X.G., Yaster, M., Johns, R.A., Gauda, E.B., and Tao, Y.X. (2008). Distinct expression of synaptic NR2A and NR2B in the central nervous system and impaired morphine tolerance and physical dependence in mice deficient in postsynaptic density-93 protein. Mol Pain *4*, 45.
Luo, W., Enomoto, H., Rice, F.L., Milbrandt, J., and Ginty, D.D. (2009). Molecular identification of rapidly adapting mechanoreceptors and their developmental dependence on ret signaling. Neuron *64*, 841-856.
Madisen, L., Mao, T., Koch, H., Zhuo, J.M., Berenyi, A., Fujisawa, S., Hsu, Y.W., Garcia, A.J., 3rd, Gu, X., Zanella, S.*, et al.* (2012). A toolbox of Cre-dependent optogenetic transgenic mice for light-induced activation and silencing. Nat Neurosci *15*, 793-802.
Madisen, L., Zwingman, T.A., Sunkin, S.M., Oh, S.W., Zariwala, H.A., Gu, H., Ng, L.L., Palmiter, R.D., Hawrylycz, M.J., Jones, A.R.*, et al.* (2010). A robust and high-throughput Cre reporting and characterization system for the whole mouse brain. Nat Neurosci *13*, 133-140.
Nakatsuka, T., Ataka, T., Kumamoto, E., Tamaki, T., and Yoshimura, M. (2000). Alteration in synaptic inputs through C-afferent fibers to substantia gelatinosa neurons of the rat spinal dorsal horn during postnatal development. Neuroscience *99*, 549-556.
Rutlin, M., Ho, C.Y., Abraira, V.E., Cassidy, C., Bai, L., Woodbury, C.J., and Ginty, D.D. (2014). The cellular and molecular basis of direction selectivity of Adelta-LTMRs. Cell *159*, 1640-1651.
Tao, Y.X., Rumbaugh, G., Wang, G.D., Petralia, R.S., Zhao, C., Kauer, F.W., Tao, F., Zhuo, M., Wenthold, R.J., Raja, S.N.*, et al.* (2003). Impaired NMDA receptor-mediated postsynaptic function and blunted NMDA receptor-dependent persistent pain in mice lacking postsynaptic density-93 protein. J Neurosci *23*, 6703-6712.
Torsney, C., and MacDermott, A.B. (2006). Disinhibition opens the gate to pathological pain signaling in superficial neurokinin 1 receptor-expressing neurons in rat spinal cord. J Neurosci *26*, 1833-1843.
Uesaka, T., Nagashimada, M., Yonemura, S., and Enomoto, H. (2008). Diminished Ret expression compromises neuronal survival in the colon and causes intestinal aganglionosis in mice. J Clin Invest *118*, 1890-1898.
Vong, L., Ye, C., Yang, Z., Choi, B., Chua, S., Jr., and Lowell, B.B. (2011). Leptin action on GABAergic neurons prevents obesity and reduces inhibitory tone to POMC neurons. Neuron *71*, 142-154.
Wang, H., and Zylka, M.J. (2009). Mrgprd-expressing polymodal nociceptive neurons innervate most known classes of substantia gelatinosa neurons. J Neurosci *29*, 13202-13209.
Wang, W., Gu, J., Li, Y.Q., and Tao, Y.X. (2011). Are voltage-gated sodium channels on the dorsal root ganglion involved in the development of neuropathic pain? Mol Pain *7*, 16.
Wu, Z., Autry, A.E., Bergan, J.F., Watabe-Uchida, M., and Dulac, C.G. (2014). Galanin neurons in the medial preoptic area govern parental behaviour. Nature *509*, 325-330.
Zhao, X., Tang, Z., Zhang, H., Atianjoh, F.E., Zhao, J.Y., Liang, L., Wang, W., Guan, X., Kao, S.C., Tiwari, V.*, et al.* (2013). A long noncoding RNA contributes to neuropathic pain by silencing Kcna2 in primary afferent neurons. Nat Neurosci *16*, 1024-1031.